NUCL SCI TECH (2022) 33:21
https://doi.org/10.1007/s41365-022-01006-0

Anisotropic flow in high baryon density region

Shao-Wei Lan[1] · **Shu-Su Shi**[1]

Received: 2 December 2021 / Revised: 11 January 2022 / Accepted: 15 January 2022 / Published online: 25 February 2022

Abstract Collective flow is a powerful tool used to analyze the properties of a medium created during high-energy nuclear collisions. Here, we report a systematic study of the first two Fourier coefficients v_1 and v_2 of the proton and π^+ from Au+Au collisions in the energy range $\sqrt{s_{\rm NN}}$ = 2.11–4.9 GeV within the framework of a hadronic transport model (UrQMD). Recent results from the STAR experiment were used to test the model calculations. A mean-field mode with strong repulsive interaction is needed to reproduce the 10–40% data at 3 GeV. This implies that hadronic interactions play an important role in the collective flow development in the high baryon density region. The mean values of the freeze-out time for protons and π^+ are shifted earlier owing to the additional repulsive interactions. We predict the energy dependence of the mean values of the transverse momentum $\langle p_{\rm T}\rangle$, v_1, and v_2 for both protons and π^+ from the Au+Au collisions.

Keywords Heavy-ion collisions · QCD phase diagram · UrQMD · Collective flow · Mean-field potential

This work was supported by the National Key Research and Development Program of China (No. 2020YFE0202002) and the National Natural Science Foundation of China [Nos. 11890710 (11890711) and 12175084].

✉ Shao-Wei Lan
shaoweilan@mails.ccnu.edu.cn

Shu-Su Shi
shiss@mail.ccnu.edu.cn

[1] Key Laboratory of Quark and Lepton Physics (MOE) and Institute of Particle Physics, Central China Normal University, Wuhan 430079, China

1 Introduction

The exploration of quantum chromodynamics (QCD) phase diagrams and nuclear matter properties has been one of the most important motivations for relativistic heavy-ion collisions [1–6]. The region of high temperature and vanishing baryon chemical potential of the QCD phase diagram, where the phase transition from hadronic matter to quark–gluon plasma (QGP) [7] is a smooth crossover, has been well studied in experiments at the RHIC [8–10] and LHC [11, 12]. Theoretical calculations suggest that there may exist a critical end point in the finite baryon chemical potential region [13]. It is well known that several observables, such as directed flow [14–17] and moments of distributions of conserved charges [18], have been proposed to be sensitive to critical behavior. In the RHIC Beam Energy Scan phase I program (BES-I), the non-monotonic behavior of the net proton directed flow slope with respect to rapidity as a function of collision energy is observed, and the minimum of the distribution suggests the softest point of the equation of state (EoS) or prediction of the critical end point [19].

The collective flow [20, 21] has been extensively used to study the transverse properties of hot and dense matter created in heavy-ion collisions owing to their sensitivity to expansion dynamics. They are defined by the coefficients of the Fourier expansion of the azimuthal distribution of the emitted particles with respect to the reaction plane: [22]

$$E\frac{{\rm d}^3N}{{\rm d}^3p}=\frac{1}{2\pi}\frac{{\rm d}^2N}{p_{\rm T}{\rm d}p_{\rm T}{\rm d}y}\left[1+2\sum_{n=1}^{\infty}v_n\cos[n(\phi-\Psi_{\rm RP})]\right]. \quad (1)$$

Here, ϕ is the azimuthal angle of the emitted particles and Ψ_{RP} is the reaction plane angle. In this simulation, the reaction plane angle, Ψ_{RP}, is zero. The coefficients, v_n, can then be determined by $v_n = \langle \cos[n(\phi)] \rangle$, where the average runs over all particles in all events. The first two coefficients, v_1 and v_2, are of particular interest as they are established early during the system evolution. Recently, the STAR experiment has reported new results for collective flow at $\sqrt{s_{NN}}$ = 3 GeV [23, 24], which corresponds to a region with a high baryon density of 750 MeV [25]. The data suggest that hadronic interactions dominate the EoS in collisions at such energies. Exploring the phase structure in the high baryon density region is the main task of the second phase of the beam energy scan at the RHIC (BES-II) program [26], as well as the motivation for future facilities: such as the facility for proton and ion research (FAIR) [27], nuclotron-based ion collider facility (NICA) [28], and high-intensity heavy-ion accelerator facility (HIAF) [29, 30]. Regarding collectivity concerns, the responses of baryons and mesons are quite different. For example, we will focus on the collective measurements of protons, representative of baryons, and π^+s, representative of produced mesons. In the case of pions, if the effect of isospin is neglected, there should be no differences in the flow of π^+ and π^-. Calculations of Au+Au collisions from a hadronic transport model UrQMD [31, 32] will be used in this study.

This paper is organized as follows: The basic features of the UrQMD model are briefly discussed in Sect. 2. In Sect. 3, we present a v_1 and v_2 comparison between the UrQMD calculations and recent STAR preliminary results at $\sqrt{s_{NN}}$ = 3 GeV. The results of the energy dependence of v_1 and v_2 from UrQMD are also discussed. Finally, a summary is provided in Sect. 4.

2 The UrQMD model

The ultra-relativistic quantum molecular dynamics model (UrQMD) [31, 32] is a microscopic transport model for simulating the process of relativistic heavy-ion collisions. It has been widely and successfully used for studying pp, pA, and AA collisions in heavy-ion collision physics over a broad energy range from a few GeV to CERN LHC energies. The particle production in UrQMD is similar to other transport models, which include resonance excitation and decay, as well as string dynamics and strangeness exchange reactions. The propagation of these hadrons and their exacted states is based on binary elastic and inelastic scattering, in which the scattering cross sections are obtained from experimental data and models. The cascade version of the UrQMD model successfully describes the particle production, as well as directed flow measurements in heavy-ion collisions at collision energies $\sqrt{s_{NN}} > 7$ GeV [33, 34]. However, at lower collision energies, it is necessary to include the mean-field potential to describe the collective flow in the high baryon density region [35–39]. A baryonic Skyrme potential [35, 36], based on the relative baryon density, is popularly used for heavy-ion collisions, which defines the nuclear EoS:

$$U = \alpha\left(\frac{\rho}{\rho_0}\right) + \beta\left(\frac{\rho}{\rho_0}\right)^{\gamma}. \quad (2)$$

Here, ρ and ρ_0 are the baryon density in the ground state and baryon density, respectively. By changing the parameters α, β, and γ, the stiffness of the nuclear EoS can be controlled. In this study, the parameters α, β, and γ are -124MeV, 71 MeV, and 2, respectively, corresponding to a nuclear incompressibility of κ = 380 MeV. This value of κ was also used in this study [38], which is consistent with the HADES collective flow measurements at $\sqrt{s_{NN}}$ = 2.4 GeV [40]. Note that the value of κ depends on the collision energy and can be model dependent. As discussed in Ref. [39, 41–44], the extracted values of κ are below 300 MeV for Au+Au collisions at lower energies. The momentum-dependent potential is not included in the mean field in this study.

In this work, we use version 3.4 of the UrQMD model to generate Monte Carlo event samples of Au+Au collisions at center of mass energies of $\sqrt{s_{NN}}$ = 2.11, 2.22, 2.32, 2.4, 2.51, 2.7, 2.86, 3.0, 3.5, 4.5, and 4.9 GeV, corresponding to beam kinetic energies of 0.5, 0.7, 1.0, 1.23, 1.5, 2.0, 2.5, 2.91, 4.65, 8.9, and 11 GeV per nucleon, respectively. Both cascade and mean-field modes of UrQMD are used to systematically study the collective flow in the high baryon density region.

3 Results and discussion

Following the STAR experimental analysis procedures, the collision centrality in this study is determined by the reference multiplicity, which is the number of charged pions, kaons, and protons within the pseudorapidity range $|\eta| < 0.5$ [45]. In Fig. 1, the reference multiplicity distribution in Au+Au collisions with the UrQMD cascade version from the center-of-mass energy $\sqrt{s_{NN}}$ = 2.11–4.9 GeV is shown. These hadrons are produced more copiously at higher collision energies. The collision centrality bins for each energy can be determined by fitting the Glauber model [46]. In the following discussion, we report results from the 10–40% centrality bin where the collectivity is

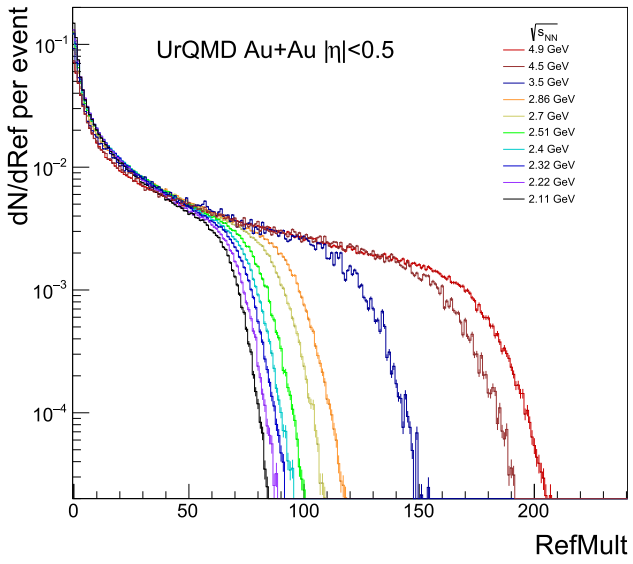

Fig. 1 (Color online) Reference multiplicity distribution in UrQMD with cascade mode in Au+Au collisions at $\sqrt{s_{NN}}$ = 2.11–4.9 GeV. Similar to the experimental setup, the charged particles were measured within $|\eta| < 0.5$

expected to have the maximum strength, especially the second order of the Fourier coefficient v_2.

According to the recent STAR collective flow measurements at $\sqrt{s_{NN}}$ = 3 GeV [23, 24], the UrQMD model results from both mean-field and cascade modes are compared with experimental data for the same centrality interval and kinematic selection criteria. Figure 2 presents the rapidity dependence of v_1 and v_2 for proton and π^+ in 10–40% centrality Au+Au collisions at $\sqrt{s_{NN}}$ = 3 GeV. The symbols denote the STAR data. The red and blue bands represent the results from the UrQMD mean-field and cascade mode, respectively. Due to the experimental acceptance, only the negative rapidity range results are shown [23].

Negative v_2 values were observed at mid-rapidity for both protons and π^+ at $\sqrt{s_{NN}}$ = 3 GeV, indicating the shadowing effect of the passing spectators. Meanwhile, the proton v_2 is positive in the forward rapidity region. For the v_1 results, a strong v_1 signal was observed compared to the high-energy results [47]. The proton v_1 increases from the forward to mid-rapidity region, whereas π^+ v_1 exhibited the opposite trend. The standard UrQMD cascade mode failed to describe the experimental data. However, by including the mean-field potential, the UrQMD results reproduce the rapidity dependence and negative v_2 values at mid-rapidity for both protons and π^+. These agreements between the experimental data and UrQMD calculations with mean-field potential imply that hadronic interactions play an important role in the collective flow development at such collision energies. Similar to Fig. 2, we present the p_T dependence of v_1 and v_2 for protons and π^+ in 10–40% centrality Au+Au collisions at $\sqrt{s_{NN}}$ = 3 GeV in Fig. 3. The mid-rapidity range of $-0.5 < y < 0$ for protons and π^+ are used in this analysis, which is consistent with the STAR experimental selection. Both v_1 and v_2 are negative and decrease with increasing p_T. Again, the red bands shown in the figure indicate the UrQMD results with mean-field potential, which can reproduce the p_T dependence and qualitatively describe the experimental data. However, quantitative differences are visible in some p_T bins for both protons and π^+.

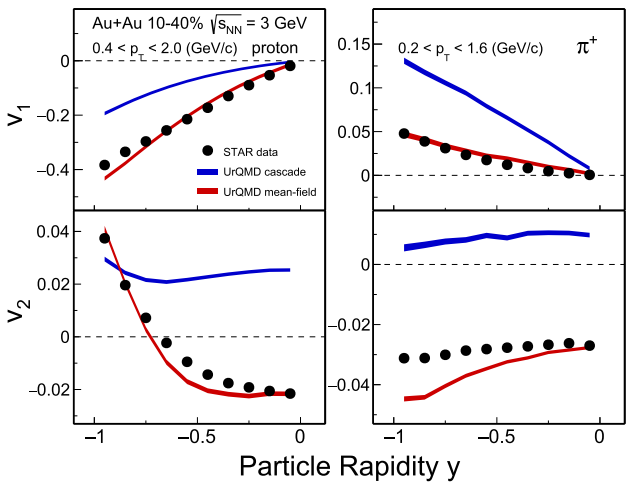

Fig. 2 (Color online) Rapidity dependence of v_1 (top panel) and v_2 (bottom panel) of the proton and π^+ in the 10–40% centrality Au+Au collision at $\sqrt{s_{NN}}$ = 3 GeV. The symbols denote STAR data. The red and blue bands represent the results from the UrQMD mean-field and cascade mode, respectively

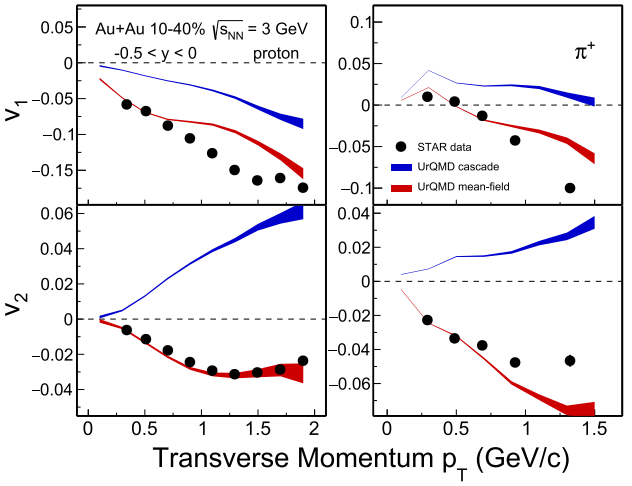

Fig. 3 (Color online) Transverse momentum dependence of v_1 (top panel) and v_2 (bottom panel) of the proton and π^+ in the 10–40% centrality Au+Au collision at $\sqrt{s_{NN}}$ = 3 GeV. The symbols denote STAR data. The red and blue bands represent the results from the UrQMD mean-field and cascade mode, respectively

We systematically studied the mean-field potential effect on the particle production, directed flow, and elliptic flow development in the high baryon density region. The particle production yield as a function of kinetic freeze-out time for protons and π^+ in 3 GeV Au+Au central collisions (0–10%) at mid-rapidity ($|y| < 0.5$) is presented in Fig. 4. The red and blue lines represent the results from the UrQMD mean-field and cascade modes, respectively. Note that these two distributions were normalized by the number of events. Overall, hadrons are produced mostly during kinetic freeze-out in the time interval 10–25 fm/c. The mean value of the distribution is shown in each panel using the corresponding colors. It can be seen that the mean value from the mean-field version is smaller than that of the cascade version. This can be explained by the larger pressure generated by the density-dependent fields, which drives the strong expansion. Thus, these hadrons are pushed outside the system and freeze out earlier than those from the cascade mode.

To quantify the strength of directed flow at mid-rapidity, a linear fit is employed to extract the slope of the $v_1(y)$ distribution [19, 47], as shown in Fig. 2. The directed flow is exactly zero at $y = 0$ owing to the momentum conservation effect. Figure 5 presents the v_1 slopes $\mathrm{d}v_1/\mathrm{d}y|_{y=0}$ and elliptic flow v_2 at mid-rapidity as a function of kinetic freeze-out time (t) for proton and π^+ in 3 GeV Au+Au mid-central collisions (10–40%); the red and blue bands represent the results from the UrQMD mean-field and cascade mode, respectively. Both v_1 and v_2 are established in the very early stage of the system evolution and show a rapid increase for $t \lesssim 15$ fm/c. They then increased slightly with increasing freeze-out time. As can be seen in the figure, the v_1 values for the mid-rapidity proton and pion start from below zero before turning into positive values at a later time, as experimentally observed. Owing to the baryonic mean field, at $t \sim 15$ fm/c, the v_1 slope for the proton is much larger than that of π^+, especially in the results for the mean-field mode. Conversely, while the

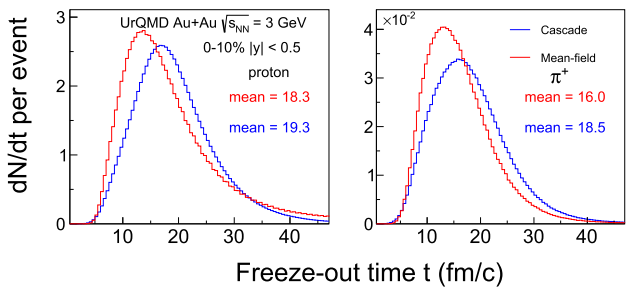

Fig. 4 (Color online) Particle production yield as a function of freeze-out time for proton (left panel) and π^+ (right panel) from UrQMD 3 GeV 0–10% Au+Au collisions. The red and blue lines represent the results from the mean-field and cascade modes, respectively

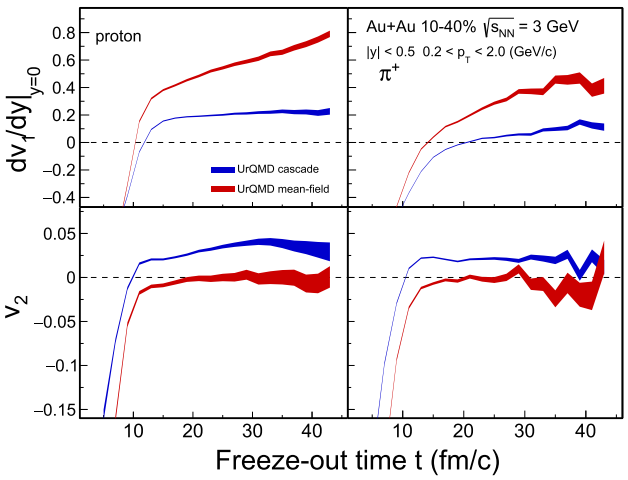

Fig. 5 (Color online) v_1 slopes ($\mathrm{d}v_1/\mathrm{d}y|_{y=0}$) and v_2 at mid-rapidity as a function of freeze-out time for proton (left panel) and π^+ (right panel) from UrQMD 3 GeV 10–40% Au+Au collisions. The red and blue bands represent the results from the mean-field and cascade modes, respectively

cascade predicts an in-plane expansion, for example, positive v_2 for both protons and pions, the mean field tends to keep the incoming nucleons together. As a result, shadowing seems to be sustained throughout the collision period, leading to negative values of v_2 and out-of-plane expansion at this energy. In short, compared to the cascade mode, the mean-field potential provides a stronger expansion in the $x - z$ plane (v_1) and an effective blocking that leads to the expansion in the $y - z$ plane (v_2) in Au+Au collisions at 3 GeV.

The mean transverse momentum $\langle p_\mathrm{T} \rangle$ as a function of collision energy $\sqrt{s_\mathrm{NN}}$ at a mid-rapidity of $|y| < 0.5$ for protons and π^+ in UrQMD 10–40% Au+Au collisions is shown in Fig. 6. The red and blue symbols represent the results from the cascade and mean-field modes, respectively. It can be observed that $\langle p_\mathrm{T} \rangle$ increases with increasing collision energy for both particle species owing to the higher energies distributed in the transverse direction. The mean-field potential slightly increases $\langle p_\mathrm{T} \rangle$ for all particles as a result of the increased radial flow. The increase in $\langle p_\mathrm{T} \rangle$ is greater for heavier particle protons. The enhancement in the mean-field mode is due to the more repulsive interactions in the high baryon density region.

We will now discuss the energy dependence of directed and elliptic flows from UrQMD and compare this with world experimental data. Figure 7 shows the energy dependence of the mid-rapidity slope of directed flow ($\mathrm{d}v_1/\mathrm{d}y|_{y=0}$) in 10–40% centrality Au+Au collisions. The transverse momentum range in the UrQMD calculations for proton and π^+ is $0.4 < p_\mathrm{T} < 2.0$ GeV/c and $0.2 < p_\mathrm{T} < 1.6$ GeV/c, respectively, which is consistent with the STAR 3 GeV results [23]. The black symbols denote the world

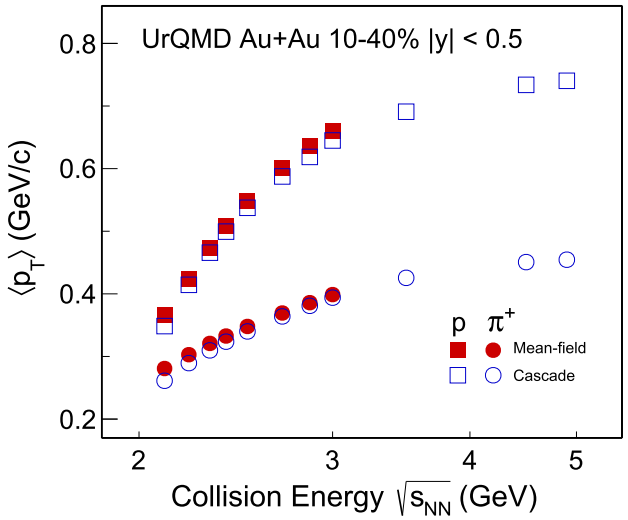

Fig. 6 (Color online) Mean transverse momentum $\langle p_T \rangle$ as a function of collision energy for proton (squares) and π^+ (circles) from UrQMD 10–40% Au+Au collisions. The red and blue symbols represent the results from the mean-field and cascade modes, respectively

experimental data [23, 48, 49]. The red and blue symbols represent the calculations from the UrQMD mean-field and cascade modes, respectively. For the π^+ v_1 and v_2 measurements, only the STAR results from $\sqrt{s_{NN}}$ = 3 and 4.5 GeV are available. The proton $dv_1/dy|_{y=0}$ values increase with decreasing collision energy for both the UrQMD cascade and mean-field calculations, while the mean-field potential significantly enhances the $dv_1/dy|_{y=0}$ values, allowing comparison with the experimental data for both protons and π^+. However, there are still some differences relating to the choice of the p_T range. As we can see in Fig. 2, v_1 has a strong p_T dependence at such a low energy.

The energy dependence of the elliptic flow at mid-rapidity in 10–40% centrality Au+Au collisions is shown in Fig. 8. The black symbols denote the world experimental data [23, 49, 50]. Both the sign and absolute value of v_2 reflect the medium properties. v_2 increases as a function of the collision energy. The results from the cascade mode are always above the results from the mean-field mode, but both converge at a high energy of approximately 5 GeV. At approximately 2.4 GeV, the proton v_2 has already changed from a negative to positive value in the cascade mode, and the change occurs at a much higher energy in the case of the mean-field calculation. According to world data, the proton elliptic flow transits from in-plane expansion to out-of-plane expansion at $\sqrt{s_{NN}} \sim 3.6$ GeV as a result of the shadowing effect, where particles are blocked in the reaction plane by the spectators and are emitted mainly in the out-of-plane direction. In Fig. 8, the UrQMD calculations with the mean-field potential qualitatively describe the experimental data for both protons and π^+ and are quantitatively consistent with the data for $\sqrt{s_{NN}} < 3.6$ GeV.

4 Summary

A hadronic transport model, UrQMD, was employed to study the directed and elliptic flows in the high baryon density region. The model provides a good description of the recent STAR results of 10–40% Au+Au collisions at $\sqrt{s_{NN}}$ = 3 GeV by including the mean-field potential. This indicates that hadronic interactions play an important role in the collective flow development in the high baryon density region. Other measurements from the 3 GeV

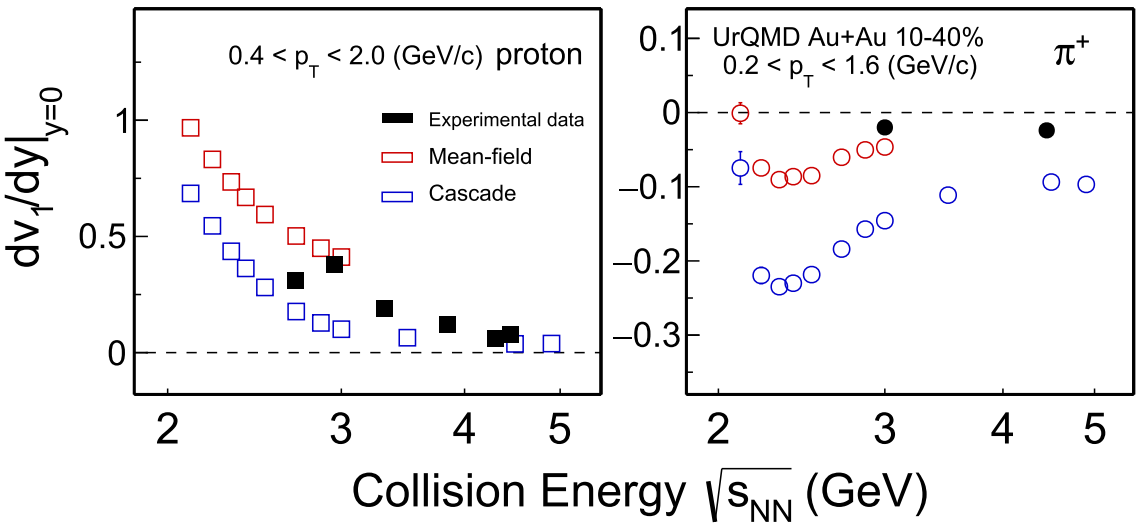

Fig. 7 (Color online) v_1 slopes ($dv_1/dy|_{y=0}$) at mid-rapidity as a function of collision energy for proton (left panel) and π^+ (right panel) from UrQMD 10–40% Au+Au collisions. The red and blue symbols represent the results from the mean-field and cascade modes, respectively. World experimental data are represented by black symbols

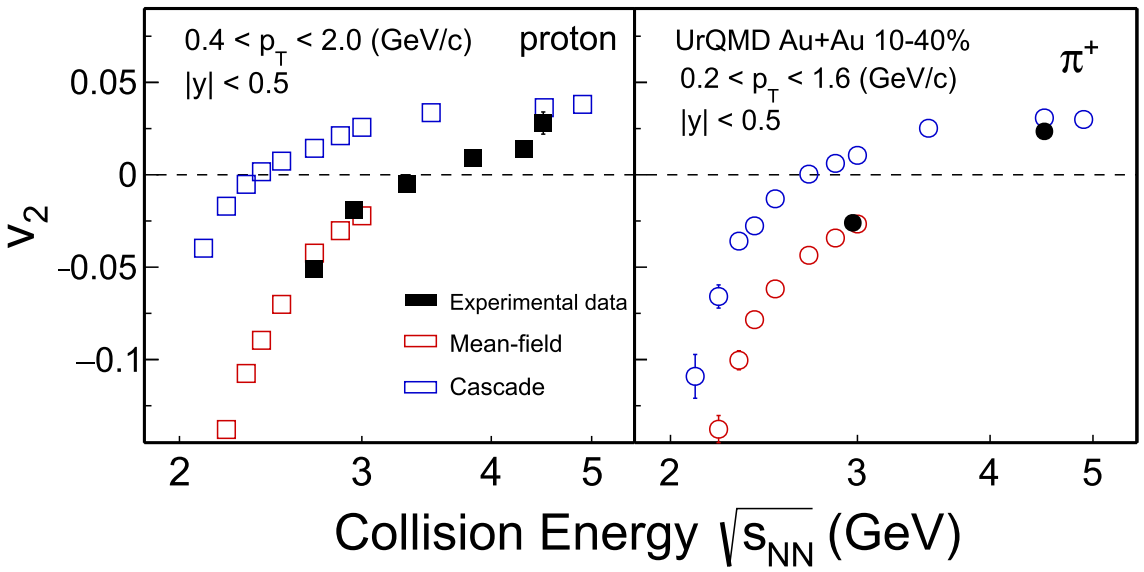

Fig. 8 (Color online) Similar to Fig. 7: v_2 at mid-rapidity as a function of the collision energy for protons (left panel) and π^+ (right panel) from UrQMD to 10–40% Au+Au collisions

Au+Au collisions, including strangeness production [51] and high moments of protons [52], also suggest that hadronic interactions dominate the dynamics in the high baryon density region.

The results of the time evolution of directed and elliptic flows show that the collective flow is fully developed at $\sim 10 - 15$ (fm/c).

The mean-field potential slightly enhances $\langle p_T \rangle$ because of the stronger radial expansion and shifts the freeze-out to an earlier time. In addition, compared to the cascade mode, the mean-field option delays the proton v_2 crossing zero as a function of collision energy, from $\sqrt{s_{NN}} = 2.5$ to 3.5 GeV. A negative or positive v_2 corresponds to an out-of-plane or in-plane expansion, respectively.

These results will be useful for understanding experimental data from upcoming experimental facilities focused on the high baryon density region.

Acknowledgements The authors thank Dr. J. Steinheimer and Dr. N. Xu for exciting discussions and the computing code.

Authors' contributions All authors contributed to the study conception and design. Material preparation, data collection, and analysis were performed by Shao-Wei Lan and Shu-Su Shi. The first draft of the manuscript was written by Shao-Wei Lan, and all authors commented on previous versions of the manuscript. All authors read and approved the final manuscript.

References

1. A. Bzdak, S. Esumi, V. Koch et al., Mapping the phases of quantum chromodynamics with beam energy scan. Phys. Rep. **853**, 1–87 (2020). https://doi.org/10.1016/j.physrep.2020.01.005
2. X. Luo, S. Shi, Y. Zhang et al., A study of the properties of the QCD phase diagram in high-energy nuclear collisions. Particles **3**, 278–307 (2020). https://doi.org/10.3390/particles3020022
3. C. Shen, L. Yan, Recent development of hydrodynamic modeling in heavy-ion collisions. Nucl. Sci. Tech. **31**, 122 (2020). https://doi.org/10.1007/s41365-020-00829-z
4. Z. Tang, W. Zha, Y. Zhang, An experimental review of open heavy flavor and quarkonium production at RHIC. Nucl. Sci. Tech. **31**, 81 (2020). https://doi.org/10.1007/s41365-020-00785-8
5. Z. Lin, L. Zheng, Further developments of a multi-phase transport model for relativistic nuclear collisions. Nucl. Sci. Tech. **32**, 113 (2021). https://doi.org/10.1007/s41365-021-00944-5
6. S. Wu, C. Shen, H. Song, Dynamically exploring the QCD matter at finite temperatures and densities: a short review. Chin. Phys. Lett. **38**, 081201 (2021). https://doi.org/10.1088/0256-307X/38/8/081201
7. E. Shuryak, Quark-gluon plasma and hadronic production of leptons, photons and psions. Phys. Lett. B **78**, 150–153 (1978). https://doi.org/10.1016/0370-2693(78)90370-2
8. A. Adare, S. Afanasiev, C. Aidala et al., (PHENIX Collaboration), Scaling properties of azimuthal anisotropy in Au + Au and Cu + Cu collisions at $\sqrt{s_{NN}}$ = 200 GeV. Phys. Rev. Lett. **98**, 162301 (2007). https://doi.org/10.1103/PhysRevLett.98.162301
9. B.I. Abelev, M.M. Aggarwal, Z. Ahammed et al., (STAR collaboration), partonic flow and ϕ-meson production in Au + Au collisions at $\sqrt{s_{NN}}$ = 200 GeV. Phys. Rev. Lett. **99**, 112301 (2007). https://doi.org/10.1103/PhysRevLett.99.112301
10. L. Adamczyk, J.K. Adkins, G. Agakishiev et al., (STAR collaboration), measurement of D^0 azimuthal anisotropy at midrapidity in Au + Au collisions at $\sqrt{s_{NN}}$ = 200 GeV. Phys. Rev. Lett. **118**, 212301 (2017). https://doi.org/10.1103/PhysRevLett.118.212301
11. K. Aamodt, B. Abelev, A. Abrahantes Quintana *et al.* (ALICE Collaboration), Higher harmonic anisotropic flow measurements of charged particles in Pb-Pb collisions at $\sqrt{s_{NN}}$ = 2.76 TeV. Phys. Rev. Lett. **107**, 032301 (2011). https://doi.org/10.1103/PhysRevLett.107.032301
12. G. Aad, B. Abbott, J. Abdallah *et al.* (ATLAS Collaboration), Measurement of the azimuthal anisotropy for charged particle production in $\sqrt{s_{NN}}$ = 2.76 TeV lead-lead collisions with the

ATLAS detector. Phys. Rev. C **86**, 014907 (2012). https://doi.org/10.1103/PhysRevC.86.014907
13. Z. Han, B. Chen, Y. Liu, Critical temperature of deconfinement in a constrained space using a bag model at vanishing baryon density. Chin. Phys. Lett. **37**, 112501 (2020). https://doi.org/10.1088/0256-307x/37/11/112501
14. H. Stöcker, W. Greiner, High energy heavy ion collisions-probing the equation of state of highly excited hadronic matter. Phy. Rep. **137**, 277–392 (1986). https://doi.org/10.1016/0370-1573(86)90131-6
15. Y. Nara, H. Niemi, J. Steinheimer et al., Equation of state dependence of directed flow in a microscopic transport model. Phys. Lett. B **769**, 543–548 (2017). https://doi.org/10.1016/j.physletb.2017.02.020
16. Y. Nara, H. Niemi, A. Ohnishi et al., Examination of directed flow as a signature of the softest point of the equation of state in QCD matter. Phys. Rev. C **94**, 034906 (2016). https://doi.org/10.1103/PhysRevC.94.034906
17. C. Zhang, J. Chen, X. Luo et al., Beam energy dependence of the squeeze-out effect on the directed and elliptic flow in Au + Au collisions in the high baryon density region. Phys. Rev. C **97**, 064913 (2018). https://doi.org/10.1103/PhysRevC.97.064913
18. J. Adam, L. Adamczyk, J.R. Adams et al., (STAR collaboration), nonmonotonic energy dependence of net-proton number fluctuations. Phys. Rev. Lett. **126**, 092301 (2021). https://doi.org/10.1103/PhysRevLett.126.092301
19. L. Adamczyk, J.K. Adkins, G. Agakishiev et al., (STAR collaboration), beam-energy dependence of the directed flow of protons, antiprotons, and Pions in Au+Au collisions. Phys. Rev. Lett. **112**, 162301 (2014). https://doi.org/10.1103/PhysRevLett.112.162301
20. H. Sorge, Elliptical flow: a signature for early pressure in ultra-relativistic nucleus-nucleus collisions. Phys. Rev. Lett. **78**, 2309 (1997). https://doi.org/10.1103/PhysRevLett.78.2309
21. J.-Y. Ollitrault, Anisotropy as a signature of transverse collective flow. Phys. Rev. D **46**, 229 (1992). https://doi.org/10.1103/PhysRevD.46.229
22. A.M. Poskanzer, S.A. Voloshin, Methods for analyzing anisotropic flow in relativistic nuclear collisions. Phys. Rev. C **58**, 1671 (1998). https://doi.org/10.1103/PhysRevC.58.1671
23. M. Abdallah *et al.* (STAR Collaboration), Disappearance of partonic collectivity in $\sqrt{s_{NN}}$ = 3 GeV Au+Au collisions at RHIC. arXiv:2108.00908 [nucl-ex]
24. S. Lan, *for the STAR Collaboration* (Anisotropic Flow Measurements of Identified Particles in the STAR Experiment, CPOD, 2021). arXiv:2109.10983 [nucl-ex]
25. J. Cleymans, H. Oeschler, K. Redlich et al., Comparison of chemical freeze-out criteria in heavy-ion collisions. Phys. Rev. C **73**, 034905 (2006). https://doi.org/10.1103/PhysRevC.73.034905
26. STAR Note 0598: BES-II whitepaper: studying the phase diagram of QCD matter at RHIC. http://drupal.star.bnl.gov/STAR/starnotes/public/sn0598
27. T. Ablyazimov, A. Abuhoza, R.P. Adak et al., (CBM collaboration), challenges in QCD matter physics -the scientific programme of the compressed baryonic matter experiment at FAIR. Eur. Phys. J. A **53**, 60 (2017). https://doi.org/10.1140/epja/i2017-12248-y
28. V. Kekelidze, A. Kovalenko, R. Lednicky et al., Prospects for the dense baryonic matter research at NICA. Nucl. Phys. A **956**, 846–849 (2016). https://doi.org/10.1016/j.nuclphysa.2016.03.019
29. J.C. Yang, J.W. Xia, G.Q. Xiao et al., High intensity heavy ion accelerator facility (HIAF) in China. Nucl. Instrum. Meth. B **317**, 263–265 (2013). https://doi.org/10.1016/j.nimb.2013.08.046
30. L. Lyu, H. Yi, L.M. Duan et al., Simulation and prototype testing of multi-wire drift chamber arrays for the CEE. Nucl. Sci. Tech. **31**, 11 (2020). https://doi.org/10.1007/s41365-019-0716-x
31. S.A. Bass, M. Belkacem, M. Brandstetter et al., Microscopic models for ultrarelativistic heavy ion collisions. Prog. Part. Nucl. Phys. **41**, 255 (1998). https://doi.org/10.1016/S0146-6410(98)00058-1
32. M. Bleicher, E. Zabrodin, C. Spieles et al., Relativistic hadron-hadron collisions in the ultra-relativistic quantum molecular dynamics model. J. Phys. G **25**, 1859 (1999). https://doi.org/10.1088/0954-3899/25/9/308
33. Y. Gao, F. Liu, A.H. Tang, Directed flow of transported and nontransported protons in Au + Au collisions from an ultrarelativistic quantum molecular dynamics model. Phys. Rev. C **86**, 044901 (2012). https://doi.org/10.1103/PhysRevC.86.044901
34. E.L. Bratkovskaya, M. Bleicher, M. Reiter et al., Strangeness dynamics and transverse pressure in relativistic nucleus-nucleus collisions. Phys. Rev. C **69**, 054907 (2004). https://doi.org/10.1103/PhysRevC.69.054907
35. J. J. Molitoris, H. Stöcker, Further evidence for a stiff nuclear equation of state from a transverse-momentum analysis of Ar(1800 MeV/nucleon) + KCl. Phys. Rev. C **32**, 346 (1985). https://doi.org/10.1103/PhysRevC.32.346
36. H. Kruse, B.V. Jacak, H. Stoecker, Microscopic theory of pion production and sidewards flow in heavy-ion collisions. Phys. Rev. Lett. **54**, 289 (1985). https://doi.org/10.1103/PhysRevLett.54.289
37. A.B. Larionov, W. Cassing, C. Greiner et al., Squeeze-out of nuclear matter in peripheral heavy-ion collisions and momentum-dependent effective interactions. Phys. Rev. C **62**, 064611 (2000). https://doi.org/10.1103/PhysRevC.62.064611
38. P. Hillmann, J. Steinheimer, M. Bleicher, Directed, elliptic and triangular flow of protons in Au+Au reactions at 1.23 A GeV: a theoretical analysis of the recent HADES data. J. Phys. G **45**, 085101 (2018). https://doi.org/10.1088/1361-6471/aac96f
39. Y.J. Wang, C.C. Guo, Q.F. Li et al., Determination of the nuclear incompressibility from the rapidity-dependent elliptic flow in heavy-ion collisions at beam energies 0.4A-1.0A GeV. Phys. Lett. B **778**, 207–212 (2018). https://doi.org/10.1016/j.physletb.2018.01.035
40. J. Adamczewski-Musch, O. Arnold, C. Behnke et al., (HADES Collaboration), Directed, elliptic, and higher order flow harmonics of protons, deuterons, and tritons in Au + Au collisions at $\sqrt{s_{NN}}$ = 2.4 GeV. Phys. Rev. Lett. **125**, 262301 (2020). https://doi.org/10.1103/PhysRevLett.125.262301
41. P. Danielewicz, R. Lacey, W.G. Lynch, Determination of the equation of state of dense matter. Science **298**, 1592–1596 (2002). https://doi.org/10.1126/science.1078070
42. C. Sturm, I. Böttcher, M. Dębowski et al., Evidence for a soft nuclear equation-of-state from kaon production in heavy-ion collisions. Phys. Rev. Lett. **86**, 39 (2001). https://doi.org/10.1103/PhysRevLett.86.39
43. Ch. Hartnack, H. Oeschler, J. Aichelin, Hadronic matter is soft. Phys. Rev. Lett. **96**, 012302 (2006). https://doi.org/10.1103/PhysRevLett.96.012302
44. Z. Feng, Constraining the high-density behavior of nuclear equation of state from strangeness production in heavy-ion collisions. Phys. Rev. C **83**, 067604 (2011). https://doi.org/10.1103/PhysRevC.83.067604
45. L. Adamczyk, O. Arnold, C. Behnke et al., (STAR Collaboration), Elliptic flow of identified hadrons in Au+Au collisions at $\sqrt{s_{NN}} = 7.7 - 62.4$ GeV. Phys. Rev. C **88**, 014902 (2013). https://doi.org/10.1103/PhysRevC.88.014902
46. M.L. Miller, K. Reygers, S.J. Sanders et al., Glauber modeling in high-energy nuclear collisions. Ann. Rev. Nucl. Part. Sci. **57**, 205 (2007). https://doi.org/10.1146/annurev.nucl.57.090506.123020
47. L. Adamczyk, J.R. Adams, J.K. Adkins et al., (STAR Collaboration), Beam-energy dependence of directed flow of

$\Lambda, \bar{\Lambda}, K^{\pm}, K^0_S$ and ϕ in Au + Au collisions. Phys. Rev. Lett. **120**, 062301 (2018). https://doi.org/10.1103/PhysRevLett.120.062301
48. H. Liu, N.N. Ajitanand, J. Alexander et al., (E895 collaboration), Sideward flow in au + au collisions between 2*A* and 8*A* GeV. Phys. Rev. Lett. **84**, 5488 (2000). https://doi.org/10.1103/PhysRevLett.84.5488
49. M.S. Abdallah, J. Adam, L. Adamczyk et al., (STAR Collaboration), Flow and interferometry results from Au + Au Collisions at $\sqrt{s}_{\mathrm{NN}}$ = 4.5 GeV. Phys. Rev. C **103**, 034908 (2021). https://doi.org/10.1103/PhysRevC.103.034908
50. C. Pinkenburg, N.N. Ajitanand, J.M. Alexander et al., (E895 collaboration), elliptic flow: transition from out-of-plane to in-plane emission in Au + Au collisions. Phys. Rev. Lett. **83**, 1295 (1999). https://doi.org/10.1103/PhysRevLett.83.1295
51. M. Abdallah *et al.* (STAR Collaboration), Probing Strangeness Canonical Ensemble with K^-, $\phi(1020)$ and Ξ^- Production in Au+Au Collisions at $\sqrt{s_{NN}}$ = 3 GeV. arXiv:2108.00924 [nucl-ex]
52. M. Abdallah *et al.* (STAR Collaboration), Measurements of proton high order cumulants in $\sqrt{s_{NN}}$ = 3 GeV Au+Au collisions and implications for the QCD critical point. arXiv:2112.00240 [nucl-ex]